







Development of Porous Refractory Calcium Hexaluminate (CA6) Ceramic Material from Limestone Waste

A. G. S. Costa^{a*} , M. L. Silva^b , A. C. A. Prado^c , D. B. Silva^c , T. M. B. F. Oliveira^c ,
W. B. A. Bezerra^c 

^aUniversidade Federal de Campina Grande, R. Aprígio Veloso, 882, Bairro Universitário, 58429-900 Campina Grande, PB, Brasil.

^bUniversidade Federal do Vale do São Francisco, Av. Antônio Carlos Magalhães, 510, Country Club, 48902-300 Juazeiro, BA, Brasil.

^cUniversidade Federal do Cariri, Av. Tenente Raimundo Rocha, 1639, Cidade Universitária, 63048-080 Juazeiro do Norte, CE, Brasil.

Received: December 29, 2024; Revised: March 30, 2025; Accepted: Maio 04, 2025

Calcium hexaluminate (CA6) is a refractory material with good thermal properties and intrinsic difficulty in densification. This study explored the use of Cariri Stone residue, a calcium carbonate-rich limestone from Ceará, Brazil, as a precursor for producing refractory ceramics containing this phase. X-ray diffraction and preliminary tests were conducted to determine the optimal conditions for its incorporation into ceramic refractories. The results showed that a mixture of Cariri Stone residue and alumina, with a molar ratio of 0.5 moles of calcium oxide to 6 moles of aluminum oxide, achieved the best formation of CA6 at 1500°C. Specimens calcined at 1400°C exhibited the highest apparent porosity, indicating potential for thermal insulation applications. These findings highlight the feasibility of reusing Cariri Stone residue as a precursor for producing refractory ceramics containing the CA6 phase, offering a sustainable and promising alternative.

Keywords: Refractories, Cariri Stone waste, calcium hexaluminate, processing conditions.

1. Introduction

Cariri Stone (CS; also known as *Pedra Cariri*) is a type of laminated limestone found in the municipalities of Nova Olinda (7° 5' 24.31" S, 39° 40' 45.71" W) and Santana do Cariri (7° 10' 57.55" S, 39° 44' 14.20" W), in the region known as Chapada do Araripe, in the state of Ceará (Northeast Region, Brazil). Such stone is rich in calcium carbonate (CaCO₃) and is widely used in civil construction as a decorative stone for walls, floors, and sidewalks¹. The CS is also known for its abundance of fossils, including insects, arthropods, fish, and plants, making the region a site of great scientific value².

Since the 1940s, the exploitation of CS has played a central role in the Cariri region, in southern Ceará, becoming its backbone. There is a lack of information on production, direct jobs, and generated waste in bibliographic sources. In 2007, Vidal, Fernandes and Pequeno³ stated that this crucial economic activity generated 3,000 direct and indirect jobs and that Cariri Stone's average annual production reached 80,000 tons. A study on the CS extractive industry in Nova Olinda - Ceará, Brazil, found that in 2016 the combined production of just nine companies generated more than 43,000 m³ of CS⁴.

Beyond the numbers, the extraction of Cariri Stone has played a fundamental role in sustaining local communities

economically, underscoring the magnitude and impact of this operation. Additionally, CS production is an essential source of opportunities for the region, playing an extremely important role in local and regional development⁴. In this context, the extraction of Cariri Stone is a fundamental element in the socio-economic fabric of the region, contributing significantly to its growth and prosperity.

However, despite its economic importance, this activity has contributed to the generation of a large volume of tailings due to its low level of mechanization, associated with the physical characteristics of the rocks, such as stratification in layers of varying thickness and separated by discontinuity planes, resulting in significant environmental irresponsibility⁵. The waste generated during the rock extraction and processing stages is discarded in open areas, as depicted in Figure 1, causing environmental damage and hindering the advancement of mining fronts⁶.

The volume of losses accounts for 70% of production³ and can reach 77.8%, according to other authors⁴. In 2007, 2.4 million tons of tailings were accounted for, deposited as rubble on mining fronts, roadsides, near drains and streams⁵.

The main constituent of Cariri Stone and, consequently, its waste is calcium carbonate⁵. The use of this waste as a raw material to produce various products is justified since waste can be added to a product when its composition is similar to the traditional raw material used and/or when its

*e-mail: ana.gabriela.costa@estudante.ufcg.edu.br



Figure 1. Cariri Stone Waste: Detail of fragments (a) and residue pile (b).

properties are similar to or better than existing products on the market⁷. To minimize the environmental impact of waste from Cariri Stone extraction, exploring alternatives for its reuse is essential. In this context, several studies have been conducted aiming to incorporate this waste into the production of various types of products, such as conventional concrete⁸, calcium hydroxide⁹, ceramic tiles¹⁰, and artificial stone for coatings¹¹.

All of these alternatives are viable, but new possibilities must be studied given the slower rate of utilization compared to production, as well as the need to expand the production chain and circular economy. A less-explored approach in the literature for reusing this material is its application in the production of refractory ceramics. Specifically, heating the material to temperatures between 700 and 900°C decomposes the calcium carbonate (CaCO_3) in the matrix into carbon dioxide (CO_2) and calcium oxide (CaO), imparting refractory characteristics to the final product.

Refractory materials are technical, polycrystalline ceramics, typically inorganic and polyphase. They are volumetrically stable and capable of maintaining their physical and mechanical properties at high temperatures and under severe use conditions¹². The production of different types of refractory materials depends on the nature of the raw materials and the process used. The main categories of traditional refractories include refractory clays, high-alumina, and silica¹³. Alumina-based refractories contain at least 60% by weight of Al_2O_3 and can exceed 99% in specialized formulations. This type of refractory enables the efficient production of ceramic components through various methods, such as slip casting, pressing, and injection molding, without requiring sophisticated equipment, such as controlled-atmosphere furnaces. Additionally, high-alumina refractories are highly effective in environments subject to abrasion and erosion, such as incineration processes¹⁴.

CaO's high melting point (2572°C) has allowed its use as a refractory for steel conversion since the 19th century¹⁵. However, this oxide is prone to hydration, making it difficult

to handle and process, and prone to be corroded by iron oxides during steelmaking¹⁵. One of the ways to overcome these negative points of using calcium oxide as a refractory is to combine it with other oxide(s).

In mixtures of CaO and Al_2O_3 , the lowest eutectic temperature is just under 1400°C¹⁵. Therefore, in this system, it is possible to form several refractory phases: most of them have cementitious characteristics (i.e., react with water to harden). On the other hand, the phase with a molar ratio of 6 moles of Al_2O_3 to 1 mole of CaO (i.e., calcium hexaluminate – $\text{CaAl}_{12}\text{O}_{19}$, also known as hibonite) is non-hydratable and exhibits good properties, including a high melting point (1875°C), good mechanical properties at high temperatures, resistance to densification, chemical attack and thermal shock¹⁶⁻¹⁸. This phase has an excellent toughening mechanism and positively contributes to the residual dimensional variation of the refractory¹⁴. Additionally, it has low thermal conductivity and is also resistant to densification, which increases porosity and makes it an excellent candidate for refractory applications above 1400°C¹⁶⁻¹⁹.

The CA6 compound consists of a hexagonal phase that originates by reactions at high temperatures (above 1300°C), usually by reactions of Al_2O_3 with CaO or CaCO_3 or $\text{Ca}(\text{OH})_2$ ^{16,20-23}. The production routes are varied, such as in-situ reactions²⁴, reaction sintering²⁵, solid-state¹⁸, and sol-gel²⁶. Therefore, this work aimed to investigate the possible use of Cariri Stone tailings, a material rich in CaO, in the formulation of masses for porous ceramic refractory materials, focusing on the formation of the CA6 phase, in addition to carrying out a preliminary study of the properties of the material obtained.

2. Materials and Methods

2.1. Precursors and characterization

Commercial A-2G alumina produced by Alcoa Alumínio S/A was used to prepare the formulations, as well as Cariri

Stone Waste (CSW) collected from quarries in Nova Olinda, Ceará, Brazil. Samples of CSW and alumina were characterized to assess their chemical and mineralogical properties.

The chemical composition was analyzed using the X-ray fluorescence technique (XRF; RIGAKU, ZSX Primus II, Japan), equipped with a Rh tube and 7 analyzer crystals. For the X-ray diffraction measurements of the powders, a diffractometer (XRD; PANalytical, Xpert Pro MPD, The Netherlands) was used, with a voltage of 40kV and a current of 40 mA, copper radiation ($K\alpha$) in a range of $2\theta = 10$ to 100° , a step of 0.013° and a total measurement time of 30 minutes. The mineral phases present in each of the samples were identified using the High Score Plus software, comparing the diffraction patterns with those in the Inorganic Crystal Structure Database (ICSD). The decomposition of the CSW to obtain CaO particles was studied by thermal analysis under N_2 atmosphere (TGA; SHIMADZU, TGA-50, Japan), using a heating rate of $20^\circ\text{C}/\text{min}$ over a temperature range of 25 to 1000°C . Particle size distributions were measured through a sedimentation test, as described in ABNT NBR 7181 (1984)²⁷. The morphological characterization of the surface of the materials used was carried out using scanning electron microscopy (SEM; Tescan Vega 3, USA).

2.2. Methods

2.2.1. Preparation of the mixtures

After characterizing the raw materials, in which it was possible to determine their CaO and Al_2O_3 oxide concentrations, three formulations were prepared: one with a ratio of 1 mol of CaO to 6 moles of Al_2O_3 (1:6), another with a molar excess of CaO (1.5:6) and the last with an excess of Al_2O_3 (0.5:6). In addition, 1% PVB (polyvinyl butyral) was added to the formulations to act as a binding agent. The materials were then weighed on a digital scale, mixed, and sieved (ABNT, 200 mesh, $0.075\mu\text{m}$) to achieve a homogenized formulation.

2.2.2. Reaction of the raw materials

The mixtures containing alumina and Cariri Stone residue were sintered in a Servifor SF-M1700FH furnace (Brazil) with 3-hour steps at temperatures of 1300, 1400 and 1500°C at a heating rate of $10^\circ\text{C}/\text{min}$ to produce the CA6 phase ($\text{CaO} \cdot 6\text{Al}_2\text{O}_3$). After the sintering process, the cooling step occurred slowly until room temperature was reached. Subsequently, the resulting powder was then deagglomerated in a mortar and sieved through a sieve (ABNT, 200 mesh, $0.075\mu\text{m}$). After deagglomeration of the powders, each sample was subjected to characterization by X-ray diffraction under the same conditions described previously, in a range of $2\theta = 10$ to 70° . The quantification of the phases present in the samples was carried out through Rietveld refinement of the X-ray diffraction patterns, using the MAUD (Materials Analysis Using Diffraction) software, version 2.996.

2.2.3. Specimen preparation

X-ray diffraction analysis identified the optimal formulation and temperature for obtaining the hibonite phase - CA6. Consequently, specimens were prepared using this formulation, then sintered and subjected to preliminary physical characterization tests. To prepare the specimens, stoichiometric calculations were first performed to determine the appropriate mass percentage of each raw material relative to the desired product quantity. Therefore, 409 grams of mixture containing a mass percentage of 92.40% alumina and 7.60% waste was weighed. Homogenization was carried out dry employing mechanical agitation using an eccentric ball mill for 5 hours. After homogenization, the samples were prepared by uniaxial pressing, with a 7.0% solution of 0.50% (w/w) carboxymethylcellulose (CMC) added to enhance the strength of the specimens during the pre-burning stages. Specimens were formed using a hydraulic press with a 15-ton capacity, applying a pressure of 49 MPa to each specimen. Eight specimens were prepared in total in a rectangular metallic matrix measuring approximately 8.0×2.5 centimeters. After the forming stage, the specimens were taken to the furnace to be fired at 1500°C and 1400°C for 3 hours, at a heating rate of 10°C per minute. After firing, the specimens were characterized by determining their water absorption, apparent porosity, apparent density, and their surfaces analyzed via scanning electron microscopy (SEM; Tescan, Vega 3, USA). A total of eight specimens were used in these tests, four of which were fired at 1500°C and the other four at 1400°C . During these tests, the initial procedure consisted of weighing the dry specimens on a scale with an accuracy of 0.01 g, to obtain the dry weight (Wd), in grams, of each one. The specimens were then immersed in water for 24 hours to determine their submerged weight (Ws) and wet weight (Ww). To determine the wet weight, each submerged specimen was removed from the water, and the excess water was dried from its surface using a damp cloth. To determine the submerged weight, it was weighed using Archimedes' principle.

3. Results and Discussion

Table 1 shows the results obtained from the chemical analysis of the precursor materials using the X-ray fluorescence technique. XRF analysis showed that the Cariri Stone Waste is rich in CaO (53.16%), has a high loss on ignition (43.58%), and also contains MgO, Fe_2O_3 , and SiO_2 in relatively much lower percentages. The presence of these oxides is justified by the fact that the sample originates from a natural rock, which can directly influence the formation and microstructure of calcium hexaluminate. According to Salomão and collaborators¹⁶, impurities and other oxides play a crucial role in the development of the CA6 microstructure. The addition

Table 1. Chemical composition of precursor materials obtained by X-ray fluorescence.

Oxide	MgO	Al_2O_3	SiO_2	P_2O_5	K_2O	CaO	MnO	Fe_2O_3	SrO	Othres	LOI	Total
Alumina	2.72	94.95	0.97	0.54	0.01	0.25	0.01	0.05	0.21	0.27	0.02	100
CSW	1.03	0.31	0.56	0.02	0.02	53.16	0.24	0.76	0.11	0.21	43.58	100

* LOI - lost of ignition

of SiO₂, for instance, in a proportion of 1–3% by weight, promotes the formation of a small amount of liquid phase, facilitating the arrangement of CA6 crystals and enhancing the densification of the material. Furthermore, the presence of other oxides in the microstructure also contributes to the formation of asymmetrical CA6 crystals¹⁶.

The commercial alumina used in this study is rich in Al₂O₃ (94.95%), has MgO and SiO₂ contents, and a low loss on ignition (LOI) of around 0.02%. The Cariri Stone Waste, on the other hand, has a high LOI value (43.58%) due to the decomposition of carbonates⁷. Using the data in Table 1, calculations were made to determine the percentages and masses of the formulations to be studied. Table 2 shows these compositions.

Figure 2 shows the diffraction patterns of the crystalline phases present in commercial alumina and Cariri Stone residue. In the alumina sample, the diffractogram shows that the predominant phase is corundum (Al₂O₃) (ICSD 26790/PDF 01-074-1081)²⁸, while the diffractogram of the residue shows that the predominant phase was calcite (CaCO₃) (ICSD 028827/PDF 01-085-0849)²⁹, accompanied by characteristic peaks of dolomite (CaMg(CO₃)₂) (ICSD 040970/PDF 01-073-2409)³⁰. These results were to be expected, given that the XRF analysis (Table 1) shows the variety of oxides in these precursors.

The thermal gravimetric analysis (TGA) curve shows that the thermal decomposition of CSW starts at a temperature of 600°C and extends to approximately 815°C (Figure 3). The loss of mass shown in the TGA curve (44.40%) was attributed to the release of CO₂ mainly due to the thermal decomposition of calcium carbonate (CaCO₃), according to the reaction: $\text{CaCO}_{3(s)} \rightarrow \text{CaO}_{(s)} + \text{CO}_{2(g)}$ ³¹. Furthermore, the shape of DTGA indicates that the thermal decomposition was initiated at a slow rate and experienced rapid decomposition with increasing temperature. This observation confirms the X-ray diffraction analysis (Figure 2), which noticeably shows that the CSW is mostly composed of the calcite crystalline phase (CaCO₃) and corroborates the results of other researchers for the same material^{32,33}.

Figure 4 illustrates the morphological analysis of the raw materials. In Figure 4(a), Cariri Stone Waste, after grinding, exhibits a highly heterogeneous composition with irregularly shaped particles. In Figure 4(b), alumina particles can be observed, appearing agglomerated, with irregular shapes and a tendency toward a spherical form. The morphological aspects observed for alumina are consistent with the morphology described by other researchers³⁴.

The largest percentage of alumina particles (approximately 75-80%) has an average size between 2.5 and 10 μm (Figure 5(a)). Therefore, this raw material has a narrow

particle size distribution. The particles of Cariri Stone residue are even smaller, with approximately 90% of them presenting average sizes smaller than 3 μm (Figure 5(b)). The dimensions of these materials are equivalent to those investigated by other authors to produce derivatives of the same target material, such as hibonite-cordierite saggar³⁵, Co²⁺ and La³⁺ doped hibonite-based pigments³⁶, hibonite-containing microspherules³⁷, cryolite-resistant refractory castables³⁸, among others. This condition is advantageous since small particles lead to more complete reactions and can also directly influence packaging, drying, firing, and final properties³⁹. Since the nature of the precursors, synthesis

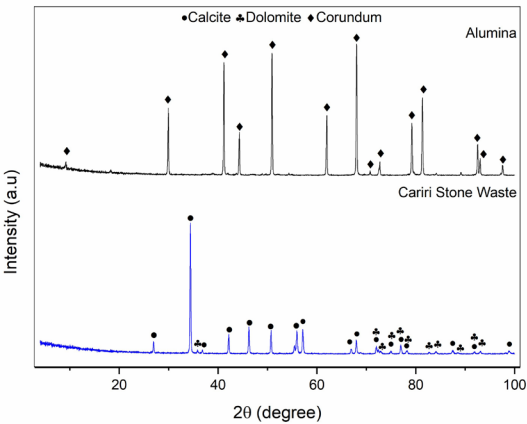


Figure 2. Diffraction patterns of crystalline phases present in commercial alumina and Cariri Stone waste.

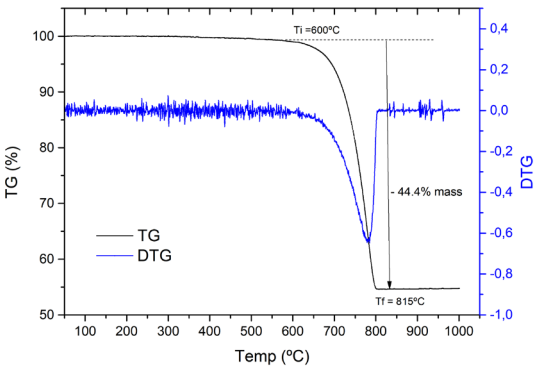


Figure 3. TGA of Cariri Stone waste showing thermal decomposition of CaCO₃.

Table 2. Formulation of the studied ceramic masses.

Sample ID	Molar ratio (CaO:Al ₂ O ₃)	Weight ratio (A/A+CSW)	Cariri Stone Waste mass (g)	Al ₂ O ₃ mass (g)
1.50C_6A	1.5 : 6	0.80	11.37	44.64
1.00C_6A	1.0 : 6	0.86	7.90	46.52
0.50C_6A	0.5 : 6	0.92	4.12	48.56

A = alumina, CSW= Cariri Stone waste

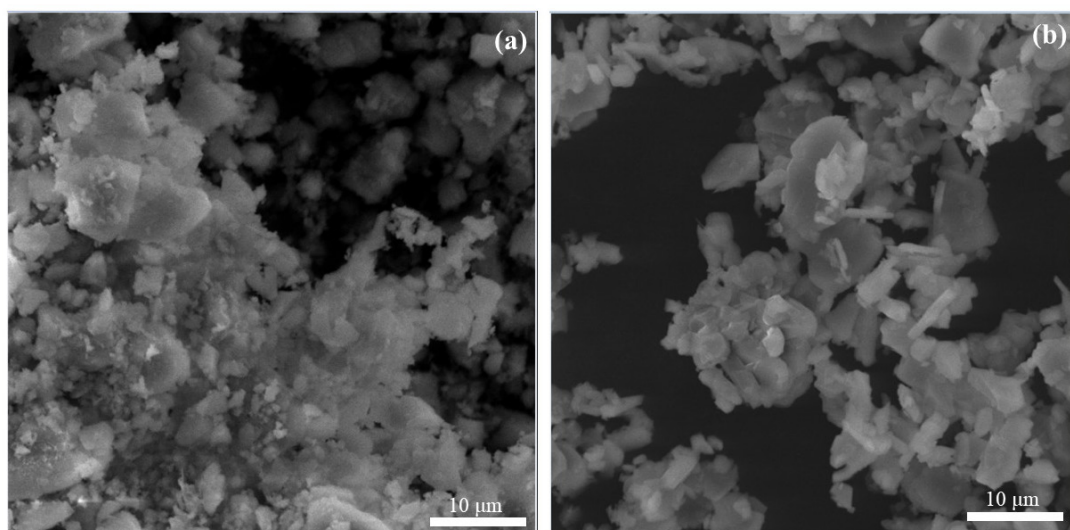


Figure 4. Scanning electron micrograph of CSW (a) and alumina (b).

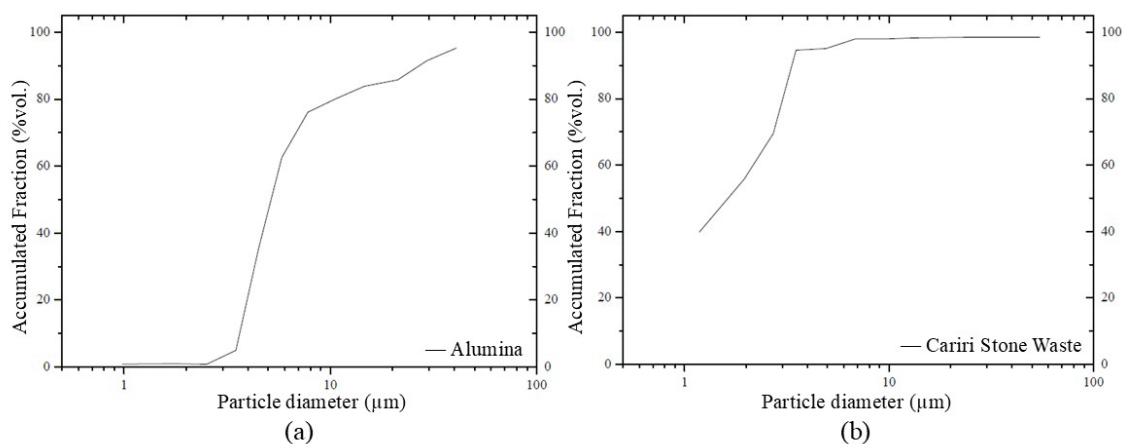


Figure 5. Particle size distribution curve for alumina (a) and CSW (b).

routes, and processing conditions of these materials were different, it is reasonable that the morphological characteristics and yield of CA6 in each case would be different, but all proposals resulted in functional ceramics.

3.1. Characterization after sintering – Crystallinity

The phases present in each sample were identified using the XRD technique. After identification, the diffractograms of the samples with a ratio of 0.5:6, 1.0:6, and 1.5:6 moles of $\text{CaO} : \text{Al}_2\text{O}_3$, fired at temperatures of 1300°C, 1400°C, and 1500°C were compared. Figure 6 (a,b,c) shows these comparisons.

In the literature, the CA6 or hibonite phase begins to form at temperatures starting from 1400°C¹⁶. In this work, the desired phase, CA6, was formed in all the molar ratios tested, starting at 1300°C with varying intensity. This can be explained by the fact that the calcium oxide-rich raw

material used had very small particle sizes, and the smaller the particles, the greater the reactivity between the raw materials during sintering. In addition to the desired phase being formed in all samples, calcium aluminate cement phases were also obtained, such as the C12A7 or mayenite phase (ICSD 06287/PDF 01-070-2144)⁴⁰ - formed in the sample with a 1.5:6 ratio, fired at 1300°C - and, above all, the CA2 or grossite phase (ICSD 16191/PDF 01-072-0767)⁴¹ - formed in all molar ratios and at all temperatures. Based on the literature, this occurrence was expected, since during heating, the raw materials react with each other, forming phases predicted by the $\text{CaO}-\text{Al}_2\text{O}_3$ binary phase diagram¹⁶. Additionally, the average size ratio between alumina and calcium sources played a crucial role in the formation of the grossite phase. In this study, the alumina particles were coarser than those of the residue. According to Oliveira and collaborators²⁰, when larger alumina particles are surrounded by fine calcium particles at temperatures around 1400°C,

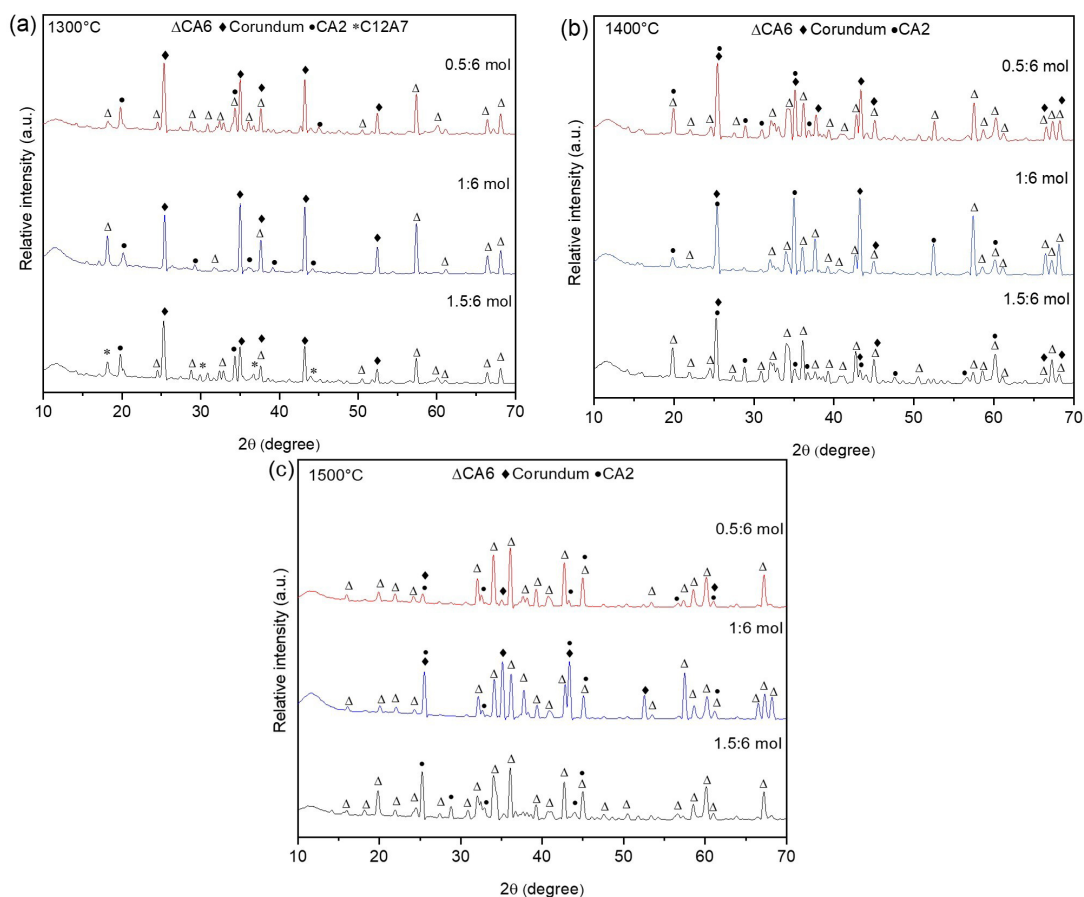


Figure 6. Comparison of diffraction patterns of samples with different molar ratios fired at 1300°C (a), 1400°C (b), and 1500°C (c).

calcium aluminate preferentially forms at the contact points, leading to the generation of a small amount of liquid phase. As the sintering process progresses, this liquid dissolves more alumina from neighboring particles, resulting in the precipitation of alumina-rich compounds, initially CA2 and later CA6.

Specifically, in the samples fired at 1300°C, the hibonite (CA6) (ICSD 34394/PDF 01-076-0665)⁴² and corundum (Al_2O_3) (ICSD 26790/PDF 01-074-1081)²⁸ phases were identified in all molar ratios, as well as the grossite (CA2) phase. At this temperature level, the corundum and grossite are predominant phases, and there was little hibonite formation. The result obtained for the sample made with the theoretical phase molar ratio (1:6 mol) showed fewer CA6 phase peaks. This result aligns with a previous research⁴³ that reports that the reaction between CaO and Al_2O_3 in a 1:6 molar ratio at 1300°C for 4 hours produced a very small amount of CA6 and higher concentration of the CA2 and Al_2O_3 phases.

At 1400°C, CA6 phase formation resulted in more intense peaks than those observed in the samples fired at 1300°C. In turn, samples fired at 1400°C also showed less intense CA6 peaks than those present in the samples fired at 1500°C. Thus, by comparing the results of the samples with varying sintering temperatures, it can be concluded that as the temperature increases, the intensity of the hibonite

phase peaks also increases, indicating a greater contribution of this phase in the studied samples. This tendency for the hibonite phase to form with increasing sintering temperature is predicted in the literature¹⁶.

Comparing the intensities of the CA6 peaks present in the three different molar ratio samples fired at 1500°C, allows us to identify the molar ratio most favorable for phase formation. When mixing the Cariri Stone waste and alumina in the theoretical molar ratio (1:6 mol) to obtain the CA6 phase, the corundum and grossite phases appear in the diffractogram as the highest intensity peaks. The hibonite phase is present, but in smaller amounts. In the composition with an excess of calcium oxide (1.5:6 mol) at 1300°C, corundum and grossite are the predominant phases, while at 1400°C, hibonite formation is promoted. At 1500°C, the most intense peaks also correspond to CA6, however, when compared to the 0.5:6 mol ratio sample, these peaks exhibit lower intensity. Therefore, since the CA6 peaks are more intense and predominant among the formed phases, the 0.5:6 mol ratio proved to be the most favorable for the formation of the desired phase at this temperature (1500°C).

It is important to highlight that CA6 formation occurs predominantly by solid-state reaction, being controlled mainly by ionic diffusion and temperature, with limited impact of the transient liquid phase. Although compaction

affects porosity and diffusion path, ion mobility is likely an even more critical condition⁴⁴, leading to similar reaction rates even with less compacted precursors. Furthermore, some studies have also indicated that the formation kinetics of CA6 depends more on the sintering temperature and time than on the initial density⁴⁵.

Table 3 presents the results of the Rietveld refinement for the sintered specimens. The sample refinement was performed using the ICSD database and corresponding ICSD reference cards N°. 06287, 16191, 34394, and 26790 to identify the crystalline phases mayenite, grossite, hibonite, and corundum, respectively. Based on the obtained data, the agreement factors for the refinements of both the standard samples and those containing residues ranged from ~12.43% to 24.06% for Rwp and ~8.02% to 9.47% for Rexp (see Table 3). The goodness-of-fit values (χ^2) were relatively low, ranging from approximately 1.55 to 2.81, indicating good refinement quality^{46,47}. Typically, the ideal χ^2 value is 1; however, higher values may be acceptable due to the possible presence of non-crystalline or minor phases⁴⁸. Additionally, typical Rwp values for refinements based on X-ray diffraction are around 20%⁴⁸. Therefore, considering that the values obtained in this study (~12.43% to 24.06%) are close to this range, they can be considered acceptable. The refinement results are consistent with the interpretations of the diffractograms, confirming the trend of increased hibonite phase formation as the sintering temperature rises. Additionally, the data indicate that at 1500°C, the most efficient formulation for maximizing the formation of this phase is the 0.5 CaO:6Al₂O₃ ratio.

3.2. Characterization of the specimens - apparent porosity, density, and water absorption

Four specimens fired at 1500°C and four fired at 1400°C, made from the 0.5CaO:6Al₂O₃ molar ratio formulation were

used in the tests. Table 4 shows the average values and standard deviations calculated for the apparent porosity of the samples. Materials fired at 1400°C exhibited higher porosity than materials fired at 1500°C. These values (45.30% at 1400°C and 42.30% at 1500°C) are higher than those found and reported by other researches^{20,49}, where samples fired at 1550 and 1600°C presented lower apparent porosity values, ranging from 25% to 30%. The composition studied in the reference works^{20,49} consisted of 85.90% alumina and 14.10% calcium carbonate by mass, while in this work samples were produced with 92.40% alumina and 7.60% calcium carbonate by mass. As apparent porosity measurements depend on the sample's composition and the firing temperature, this explains the difference observed between the values in this study and those of the reference. Another factor that may have affected the results is the pressure used in the uniaxial pressing during the specimens forming. In the reference literature⁴⁹, a pressure of 109 MPa was used, while in this study the pressure was 49 MPa. Therefore, the material produced in this work had less compression during the forming of the specimens and a lower level of densification during firing.

In addition, the apparent porosity depends on the crystalline structure of the alumina used as the raw material for the calcium hexaluminate synthesis. Oliveira and collaborators²⁰ compared the apparent porosity exhibited by formulations of calcium carbonate with ρ -Al₂O₃ and α -Al₂O₃ pressed and fired at maximum temperatures between 1550 and 1650°C. α -Al₂O₃-CaCO₃ specimens showed apparent porosity close to 30% (at three temperatures: 1550, 1600, and 1650°C), while those initially composed of ρ -Al₂O₃ and CaCO₃ showed higher apparent porosities (between 50 and 65%). In addition, these researchers²⁰ observed that ρ -Al₂O₃ transforms with increasing temperature into other transition phases up to α -Al₂O₃, generating a significant increase in the porosity of the body.

Table 3. Results for Rietveld refinement.

Sample	0.5:6 at 1300°C	0.5:6 at 1400°C	0.5:6 at 1500°C	1:6 at 1300°C	1:6 at 1400°C	1:6 at 1500°C	1.5:6 at 1300°C	1.5:6 at 1400°C	1.5:6 at 1500°C
R _{WP} (R-weighted profile)	23.26	22.12	20.63	23.28	18.74	12.43	24.06	17.62	20.50
R _{EXP} (R-expected)	8.81	9.47	8.67	8.37	8.52	8.02	8.56	8.48	8.62
χ^2 (Goodness of fit)	2.64	2.33	2.38	2.78	2.20	1.55	2.81	2.07	2.38
Phase	Weight (%)								
Corundum (rhombohedral)	37.53	32.40	3.02	60.33	51.60	56.53	39.49	6.00	-
Grossite (monoclinic)	44.28	23.42	4.48	36.43	20.46	6.20	54.48	41.97	30.26
Hibonite (hexagonal)	18.19	44.18	92.50	3.24	27.94	37.27	3.31	52.03	69.74
Mayenite (cubic)	-	-	-	-	-	-	2.72	-	-

Table 4. Average and standard deviation (SD) obtained for apparent porosity (AP), apparent density (AD) and water absorption (WA).

Temperature	Average AP(%)	SD AP (%)	Average AD (g / cm ³)	SD AD (g / cm ³)	Average WA (%)	SD WA (%)
1400°C	45.30	0.50	2.00	0.01	22.50	0.30
1500°C	42.30	0.90	2.11	0.03	20.00	0.70

When analyzing the values obtained in the water absorption, apparent porosity, and apparent density tests, the relationship between these properties is clear. Specimens fired at 1500°C had water absorption and apparent porosity values lower than those obtained for the samples fired at 1400°C, while the apparent density increased as the firing temperature rose. Since materials with denser structures have lower porosity and water absorption values, it can be concluded that such relationship between these properties was satisfied.

The theoretical density of CA6 is 3.79 g/cm³⁴³, but as materials composed of hibonite have difficulty densifying due to the morphology of their grains, the apparent densities of products composed of this phase are much lower than the actual density. An apparent density of 2.00 g/cm³ was achieved at 1400°C in this investigation was, similar to the density reported in the literature²⁶.

The average apparent density values for the specimens fired at 1500°C (2.11 g/cm³) are lower than the value obtained by Lima (2016) for the α -Al₂O₃-CaCO₃ specimens fired at 1600°C (2.58 g/cm³)⁴⁹. The parameter differences in specimens' preparation between this work and Lima's (2016) is most likely the cause of the higher apparent density in the reference.

3.3. Characterization of the specimens – Morphology

Figure 7 shows a comparison between the specimens before and after firing. There was only a slight change in the color and size of the specimens. In addition, the final microstructures of the surfaces of the samples fired at 1400°C and 1500°C are shown in Figures 8 and 9.

As can be seen, the microstructures of both samples consist of platelet-shaped structures. In Figure 8, which shows

a material with a molar ratio of 0.5:6 burned at 1400°C, the platelets appear more irregular, whereas in Figure 9, depicting a material with the same molar ratio fired at 1500°C, the platelets are equiaxed.

This platelet morphology is similar to that observed by Chen and others⁴³ for grains obtained after firing 1 mol of CaO with 6 mol of Al₂O₃ above 1400°C. These researchers⁴³ chemically analyzed the grains and the molar ratios of Al, Ca, and O are compatible with the CA6 phase.

The microstructural particularities influence the physical properties of these materials, so that the sample fired at 1500°C had a higher apparent density (g/cm³) since equiaxed particles promote a more closed/compact structure, which favors better densification. In addition, the plate shape of the CA6 grains favors the high porosity presented by the material⁵⁰.

The shape of the particles in these materials favors the formation of a low weight porous structure after sintering, which is very efficient as a thermal insulator since the closed pores in their structure reduce heat transfer due to the low thermal conductivity of the air trapped in these spaces⁵¹.

The average particle size also influences the material's microstructure. Researchers¹⁶ mixing CaCO₃ and α -Al₂O₃ concluded that the decomposition of CaCO₃ increases the distance between particles and reduces the number of effective contact points between the reactants. Since solid-state diffusion occurs at these contact points, the formation of CA6 crystals tends to be asymmetrical. Additionally, when the precursors have significantly different particle sizes, as observed in this study, imperfect contacts between Al₂O₃ and CaO arise¹⁶. In this work, this occurred because the alumina used had significantly larger particles than those of the residue.

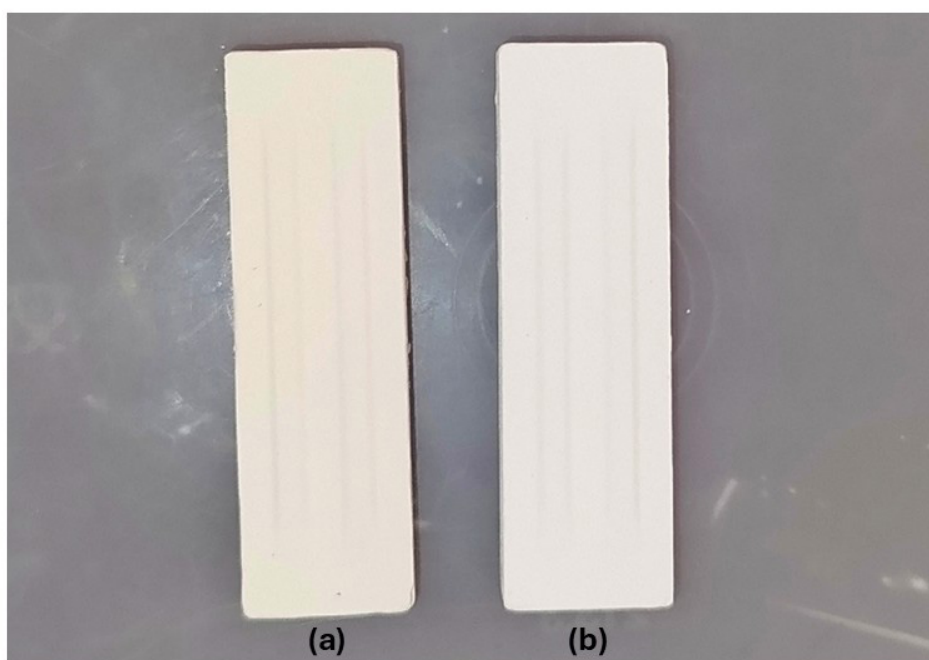


Figure 7. Test specimen before firing (a) and after firing at a temperature of 1300°C (b).

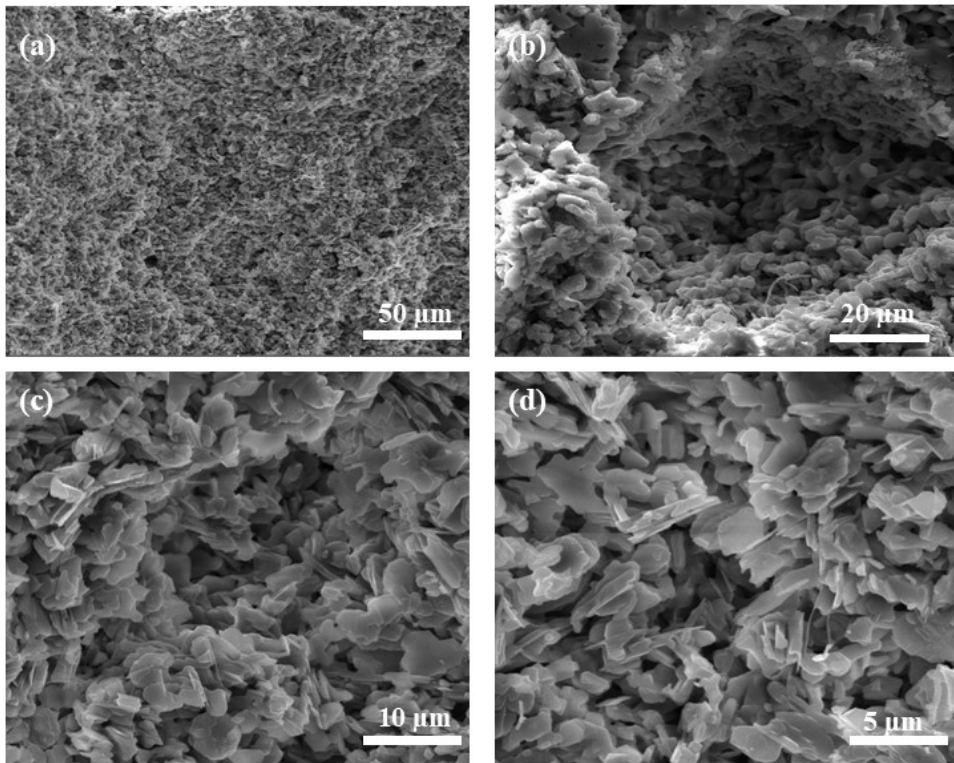


Figure 8. Microstructures of the surfaces of the samples burned for 3 hours at a temperature of 1400°C on a scale of 50 µm (a), 20 µm (b), 10 µm (c), and 5 µm (d).

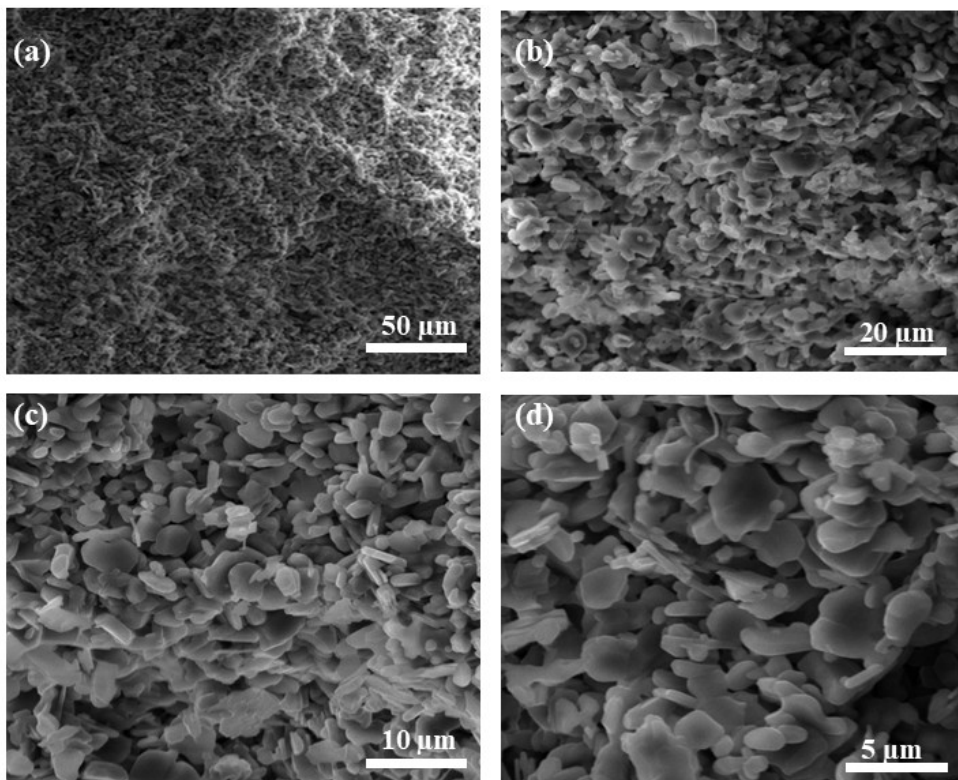


Figure 9. Microstructures of the surfaces of samples fired for 3 hours at a temperature of 1500°C on a scale of 50 µm (a), 20 µm (b), 10 µm (c), and 5 µm (d).

4. Conclusions

The Cariri Stone waste is rich in calcium oxide and, when paired with alumina, becomes an attractive raw material to be used in the production of porous refractory ceramic materials. The diffractograms and the comparisons made based on the temperatures tested showed that the intensity of the CA6 phase peaks in the samples increases as the temperature rises. Therefore, it can be seen that among the three temperatures studied (1300°C, 1400°C, and 1500°C), the temperature of 1500°C presents the best conditions for the refractory material to form calcium hexaluminate (hibonite). Also, analyzing the different formulation fired at 1500°C, the resulting diffractograms showed that the CA6 phase was formed in all the samples, but in different quantities. The formulation with a molar ratio of 0.5CaO:6Al₂O₃ proved to be the most favorable for the formation of the desired phase, exhibiting the highest relative peak intensities. Additionally, the Rietveld refinement indicated a composition of 92.5% of the CA6 phase for this ratio, confirming its predominance. Preliminary tests showed that the variation in the physical properties of apparent density, apparent porosity, and water absorption is directly related to temperature. Thus, at 1400°C, the material proved to be prone to obtaining a more porous, less dense microstructure with greater water absorption capacity. Therefore, under these conditions, the material present the most potential for use in applications that require greater thermal insulation. In summary, the results of this work are highly significant in further stimulating interest in the development of technological refractory materials, while also offering a new perspective on the sustainable use of Cariri Stone Waste.

5. Acknowledgements

The authors gratefully acknowledge the funding received from the Brazilian agencies CNPq (Proc. 308108/2020-5 and 420261/2018-4) and CAPES (Finance code 001), as well as UFCA (for the undergraduate research scholarships). The authors also thank Mariane Cibelle Marques Bezerra for kindly authorizing the use of the photographs presented in Figure 1.

6. References

1. Silva ADA. Aproveitamento de rejeito de calcário do Cariri Cearense na formulação de argamassa [dissertation]. Recife: Universidade Federal de Pernambuco; 2008.
2. Rodrigues GG. Exploração e beneficiamento da pedra Cariri nas cidades de Nova Olinda e Santana do Cariri-CE [undergraduate thesis]. Mossoró: Universidade Federal Rural do Semi-Árido; 2018.
3. Vidal FWH, Fernandes TWG, Pequeno D. Inovação tecnológica para a valorização da Pedra Cariri, CE. Rio de Janeiro: CETEM/MCTI; 2007.
4. Moraes AHM, Oliveira JFA, Marinho JLA, Silva Januário TL. Análise ambiental das atividades de mineração da pedra Cariri no município de Nova Olinda-CE. *Rev Gest Sustent Ambient*. 2020;9(2):57-73.
5. Vidal FWH, Lima MAB, Castro NF, Fernandes TWG. Aplicações industriais dos calcários do Cariri cearense. Rio de Janeiro: CETEM/MCTI; 2007.
6. Menezes RR, Melo LRL, Fonsêca FAS, Souto PM, Neves GA, Santana LNJ. Reciclagem do resíduo da serragem de calcário laminado para produção de blocos cerâmicos. *Ceramica*. 2010;63:667-72.
7. Prado ACA, Feitosa RLM, Neves MA, Taguchi SP. The influence of compositional variability of dimension stone residues on the properties of rustic porous ceramic tiles. *Ceramica*. 2023;69:23-9.
8. Moura WA, Leite MB, Bastos AJO. Avaliação do uso de resíduo de serragem de pedra Cariri (RSPC) para produção de concretos convencionais. *Ambient Constr*. 2013;13(1):7-24.
9. Alves T, Santos A, Brasileiro M, Pinheiro S, Prado A. Produção de hidróxido de cálcio a partir de resíduo da pedra Cariri. In: 22° CBECIMat: Congresso Brasileiro de Engenharia e Ciência dos Materiais; 2016 Nov 6-10; Natal, RN. Proceedings. São Paulo: Metallum Congressos Técnicos e Científicos; 2016. p. 2355-66.
10. Barroso M, Pereira F, Santos I, Melo P, Vieira F, Marinho R. Evaluation of the incorporation of Cariri stone in masses of ceramics tiles. In: 22° CBECIMat: Congresso Brasileiro de Engenharia e Ciência dos Materiais; 2016 Nov 6-10; Natal, RN. Proceedings. São Paulo: Metallum Congressos Técnicos e Científicos; 2016. p. 2368-78.
11. Bezerra AKL, Silva LA, Araújo LBR, Cabral AEB. Production and characterization of artificial stone for coating with limestone waste laminated in polymeric matrix. *Ambient Constr*. 2022;22:23-33.
12. Sako EY, Pandolfelli VC. A relação entre a corrosão e a microestrutura: a chave para o desenvolvimento de concretos refratários espinelizados de alto desempenho. *Ceramica*. 2014;60(353):127-43.
13. Sengupta P. Refractories for the chemical industries. Cham: Springer International Publishing; 2020. Chapter 2, Classification of refractories; p. 31-41.
14. Sadik C, El Amrani I-E, Albizane A. Recent advances in silica-alumina refractory: a review. *Journal of Asian Ceramic Societies*. 2014;2(2):83-96.
15. Nadachowski F. Refractories based on lime: development and perspectives. *Ceramurg Int*. 1976;2(2):55-61.
16. Salomão R, Ferreira VL, Oliveira IR, Souza ADV, Correr WR. Mechanism of pore generation in calcium hexaluminate (CA6) ceramics formed in situ from calcined alumina and calcium carbonate aggregates. *J Eur Ceram Soc*. 2016;36(16):4225-35.
17. Si Y, Li H, Sun H, Xia M, Du Y, Shang X, et al. Effects of firing temperature and Al additive on the microstructures and properties of SiC-CA6 composite refractories. *Mater Today Commun*. 2022;31:103314.
18. Xu L, Wang E, Hou X, Chen J, He Z, Liang T. Effect of incorporation of nitrogen on calcium hexaluminate. *J Eur Ceram Soc*. 2020;40(15):6155-61.
19. Costa LM, Sakihama Uehara J, Salomão R. Characterization of porous calcium hexaluminate ceramics produced from calcined alumina and microspheres of vaterite (μ -CaCO₃). *J Eur Ceram Soc*. 2018;38:5208-18.
20. Oliveira IR, Leite VMC, Lima MPVP, Salomão R. Production of porous ceramic material using different sources of alumina and calcia. *Materia*. 2015;20(3):739-46.
21. Liu J, Liu Z, Feng J, Li B, Chen J, Ren B, et al. Reaction mechanism of CA6, Al₂O₃ and CA6-Al₂O₃ refractories with refining slag. *Materials*. 2022;15:6779.
22. Salomão R, Ferreira VL, Costa LMM, Oliveira IR. Effects of the initial CaO-Al₂O₃ ratio on the microstructure development and mechanical properties of porous calcium hexaluminate. *Ceram Int*. 2018;44(2):2626-31.
23. Sako EY, Brailio MAL, Milanez DH, Brant PO, Pandolfelli VC. Microsilica role in the CA6 formation in cement-bonded spinel refractory castables. *J Mater Process Technol*. 2009;209(15):5552-7.
24. Zhang X, Liang J, Li J, Zeng Y, Hao S, Liu P, et al. The properties characterization and strengthening-toughening mechanism of Al₂O₃-CA6-MA-Ni multi-phase composites prepared by adding calcined dolomite. *Mater Charact*. 2022;186:111810.

25. Cui K, Fu T, Zhang Y, Wang J, Mao H, Tan T. Microstructure and mechanical properties of CaAl₁₂O₁₉ reinforced Al₂O₃-Cr₂O₃ composites. *J Eur Ceram Soc.* 2021;41(15):7935-45.
26. Hossain SS, Preeti J, Roy PK, Bera J. Development of dense Sr-substituted CaAl₁₂O₁₉ (CA6) ceramics synthesized by sol-gel combustion method. *J Asian Ceram Soc.* 2021;9(3):1007-14.
27. ABNT: Associação Brasileira de Normas Técnicas. NBR 7181: análise granulométrica: solo. Rio de Janeiro: ABNT; 1984.
28. Saalfeld H. Strukturuntersuchungen im system Al₂O₃-Cr₂O₃. *Z Kristallogr.* 1964;120(1-6):342-8.
29. Elliott N. A redetermination of the carbon-oxygen distance in calcite and the nitrogen-oxygen distance in sodium nitrate. *J Am Chem Soc.* 1937;59(7):1380-2.
30. Reeder R, Markgraf SJ. TEM observations and X-ray crystal-structure refinement of a twinned dolomite with a modulated microstructure. *Am Mineral.* 1986;71:795-804.
31. Karunadasa KSP, Manoratne CH, Pitawala HMTGA, Rajapakse RMG. Thermal decomposition of calcium carbonate (calcite polymorph) as examined by in-situ high-temperature X-ray powder diffraction. *J Phys Chem Solids.* 2019;134:21-8.
32. Shi Z, Luo C, Lai D, Luo T, Yang P, Li X, et al. A modified pore evolution particle model applied to CaCO₃ decomposition and CaO sintering during calcium looping CO₂ cycles. *Separ Purif Tech.* 2025;355:129733.
33. Csáki Š, Húlan T, Ondruška J, Štubňa I, Trnovcová V, Lukáč F, et al. Electrical conductivity and thermal analyses studies of phase evolution in the illite-CaCO₃ system. *Appl Clay Sci.* 2019;178:105140.
34. Oliveira AGF, Gomes UU, Lima HD, Lima MJ. Obtaining composites powders of Al₂O₃/Ni and Al₂O₃/Nb by mechanical alloying. *Mater Res.* 2019;22(5):e20190299.
35. Gan C, Zhang H, Zhao H, Zhang Y, Liu H. Effect of aggregate particle content on sintering and corrosion resistance of hibonite-cordierite saggars. *Ceram Int.* 2023;49(1):907-17.
36. Rus I, Ianoş R, Lazău R, Păcurariu C. New blue pigments based on Co²⁺ and La³⁺ doped hibonite for NIR-reflective coatings. *Mater Today Chem.* 2023;28:101391.
37. Ireland TR, Fahey AJ, Zinner EK. Hibonite-bearing microspherules: a new type of refractory inclusions with large isotopic anomalies. *Geochim Cosmochim Acta.* 1991;55(1):367-79.
38. Li Y, Zhao H, Zhang H, Yu J, Wang W, Xu J. Enhanced cryolite resistance of CA6-based refractory castables through the phase distribution of ferrotitanium slag. *Ceram Int.* 2025;51(5):6058-66.
39. Santos RC, Silva TR, Neves GA, Macedo RS, Menezes RR, Santana LN. Interação entre características de argilas e parâmetros de processamento sobre propriedades tecnológicas de corpos cerâmicos. *Cerâmica.* 2017;63(367):361-8.
40. Riffel H, Zettler F, Hass HJN. The crystal structure of Co₂(OH)AsO₄. *Neues Jahrb Mineral Monatsh.* 1975:514-7.
41. Ponomarev V, Kheiker D, Belov NJ. Crystal structure of calcium dialuminate, CA₂. *Kristallografiya.* 1971;15(6):995-1000.
42. Katsuo K. Verfeinerung der kristallstruktur von CaO·6Al₂O₃. *Neues Jahrb Miner Abh.* 1968;109(3):192-200.
43. Chen JH, Chen HY, Yan MW, Cao Z, Mi WJ. Formation mechanism of calcium hexaluminate. *Int J Miner Metall Mater.* 2016;23(10):1225-30.
44. Khajornboon J, Kosuke O, Kouichiro W, Shiono T. Control of hexagonal plate-like microstructure of in-situ calcium hexaluminate in monolithic refractories. *J Asian Ceram Soc.* 2018;6(3):196-204.
45. Sktani ZDI, Azhar AZA, Ratnam MM, Ahmad ZA. The influence of in-situ formation of hibonite on the properties of zirconia toughened alumina (ZTA) composites. *Ceram Int.* 2014;40(4):6211-7.
46. Wu E, Kisi EH, Gray EMA. Modelling dislocation-induced anisotropic line broadening in Rietveld refinements using a Voigt function. II. Application to neutron powder diffraction data. *J Appl Cryst.* 1998;31(3):363-8.
47. Oliveira HM, Lucena Lira H, Lima Santana LN. Thermal processing effects on biomass ash utilization for ceramic membrane fabrication. *Sustainability.* 2025;17(3):979.
48. Martelli MC, Mochiutti E, Lima JPO, Neves RF. Quantificação de mullita proveniente de resíduos de caulim da região amazônica: uso do método de Rietveld. *Quim Nova.* 2021;44(4):402-9.
49. Lima MPVP. Processo de obtenção por rotas alternativas de hexaluminato de cálcio microporoso como isolante térmico [thesis]. São José dos Campos: Universidade do Vale da Paraíba; 2016.
50. Pięta A, Bućko MM, Januś M, Lis J, Jonas S. Calcium hexaaluminate synthesis and its influence on the properties of CA₂-Al₂O₃-based refractories. *J Eur Ceram Soc.* 2015;35(16):4567-71.
51. Lo YW, Wei WCJ, Hsueh CH. Low thermal conductivity of porous Al₂O₃ foams for SOFC insulation. *Mater Chem Phys.* 2011;129(1):326-30.